Reaction of *Mycobacterium tuberculosis* Cytochrome P450 Enzymes with Nitric Oxide[†]

Hugues Ouellet,[‡] Jérôme Lang,[§] Manon Couture,[§] and Paul R. Ortiz de Montellano*[,‡]

Department of Pharmaceutical Chemistry, University of California at San Francisco, San Francisco, California 94158-2517, and Department of Biochemistry and Microbiology, Laval University, Quebec, Canada G1K 7P4

Received August 25, 2008; Revised Manuscript Received December 15, 2008

ABSTRACT: During the initial growth infection stage of *Mycobacterium tuberculosis* (*Mtb*), •NO produced by host macrophages inhibits heme-containing terminal cytochrome oxidases, inactivates iron/sulfur proteins, and promotes entry into latency. Here we evaluate the potential of •NO as an inhibitor of *Mtb* cytochrome P450 enzymes, as represented by CYP130, CYP51, and the two previously uncharacterized enzymes CYP125 and CYP142. Using UV−visible absorption, resonance Raman, and stopped-flow spectroscopy, we investigated the reactions of •NO with these heme proteins in their ferric resting form. •NO coordinates tightly to CYP125 and CYP142 (submicromolar) and with a lower affinity (micromolar) to CYP130 and CYP51. Anaerobic reduction of the ferric−NO species with sodium dithionite led to the formation of two spectrally distinct classes of five-coordinate ferrous−NO complexes. Exposure of these species to O_2 revealed that the ferrous−NO forms of CYP125 and CYP142 are labile and convert back to the ferric state within a few minutes, whereas ferrous CYP130 and CYP51 bind •NO almost irreversibly. This work clearly indicates that, at physiological concentrations ($\approx$1 μM), •NO would impair the activity of CYP130 and CYP51, whereas CYP125 and CYP142 are more resistant. Selective P450 inhibition may contribute to the inhibitory effects of •NO on *Mtb* growth.

Mycobacterium tuberculosis (*Mtb*)[1] continues to be an enormous threat to human health. Indeed, *Mtb* infects over 1.8 billion people worldwide and causes 1.5 million deaths per year. In immunocompetent individuals, the innate and adaptive arms of the immune system are relatively efficient in containing and killing *Mtb*. It is estimated that of 100 people newly infected with the tubercle bacilli, only about 5−10 individuals will develop tuberculosis over their lifetime (*1*). Host cells that are protective against *Mtb* include macrophages, dendritic cells, T-lymphocytes, and airway epithelial cells (*2*). The production of reactive oxygen intermediates and reactive nitrogen intermediates by innate immune cells is considered to be a relatively effective host-defense mechanism against microbial pathogens (*3*). For instance, exposure to •NO at low concentrations, e.g., <100 ppm, killed more than 99% of *Mtb* in culture (*4*).

The potential mechanisms by which •NO may affect antimicrobial activity are numerous. •NO and other reactive nitrogen intermediates (RNI) can modify bacterial DNA, protein, and lipids at both the microbial surface and intracellularly. •NO can also deaminate as well as directly damage bacterial DNA, generating abasic sites and strand breaks (*5*). Other potential mechanisms of killing by •NO include interaction with accessory protein targets such as iron−sulfur groups, heme group, and thiols, resulting in enzymatic inactivation or other protein malfunctions (*6*). •NO also combines at a near diffusion-limited rate with superoxide produced by respiring cells to form the highly oxidizing agent peroxynitrite (*7*). Peroxynitrite can mediate nitration of tyrosine residues, and therefore has a potential, for instance, of disrupting tyrosine phosphorylation-dependent signaling pathways (*8*).

A number of studies have implicated •NO as a mediator responsible for the decrease of cytochrome P450-dependent metabolism in human liver (*9, 10*) and suggest that the binding of •NO to the prosthetic heme of the enzyme might inhibit bacterial cytochrome P450 (P450) activities as well. Sequencing of the *Mtb* genome revealed the existence of an extraordinary array of 20 P450 enzymes, all of which are potential targets for inhibition by •NO (*11*) and at least several of which are essential for bacterial survival or pathogenicity. The location of P450-encoding genes on the *Mtb* chromosome provides little insight into their biological function, but physiological roles have been proposed for a few *Mtb* P450s, including a role in fatty acid metabolism for CYP132 and in mycolic acid or polyketide metabolism for CYP121 (*12*). *Mtb* CYP51, like its eukaryotic homologues, catalyzes 14α-demethylation of lanosterol (*13*). However, there is no evidence for the presence of a complete sterol biosynthetic pathway in *Mtb*. Instead, CYP51 may be involved in the metabolism of a host steroid. CYP142 and CYP125 are of particular interest because they are part of a chromosomal

[†] This work was supported by National Institutes of Health Grant AI074824.

* To whom correspondence should be addressed. Telephone: (415) 476-2903. Fax: (415) 502-4728. E-mail: ortiz@cgl.ucsf.edu.

[‡] University of California at San Francisco.

[§] Laval University.

[1] Abbreviations: *Mtb*, *Mycobacterium tuberculosis*; RNI, reactive nitrogen intermediates; P450, cytochrome P450; 5c, five-coordinate; 6c, six-coordinate; NOS, nitric oxide synthase; nNOS, neuronal isoform of NOS; iNOS, inducible isoform of NOS; eNOS, endothelial isoform of NOS.

10.1021/bi801595t CCC: $40.75
Published on Web 01/15/2009

DNA region found in the genome of *Mtb* and a related actinomycete *Rhodococcus* sp. strain RHA1. This large regulon, which bears several genes potentially involved in the degradation of lipids such as cholesterol, has been reported to be essential for host infection by *Mtb* (*14*). Moreover, CYP125 was recently shown to be essential for infection in mice and is induced within the macrophage (*15, 16*). To date, only CYP121, CYP130, and CYP51 have been characterized at the protein level, and crystal structures have been obtained for both the ligand-free and inhibitor-bound forms of these three proteins (*17*−*20*).

In this work, we report for the first time cloning and expression of the *Mtb cyp125* and *cyp142* genes in *Escherichia coli* cells, leading to the purification and preliminary characterization of these new P450 enzymes. Ferric CYP142, CYP125, and CYP51 reversibly bind •NO with moderate to high affinity, making them plausible targets for this natural inhibitor. The reduction of the ferric−NO complexes resulted in the formation of two classes of ferrous−NO complexes that exhibit different reactivity upon exposure to O_2. Indeed, we show here that CYP130 and, to a smaller extent, CYP51 are susceptible to almost irreversible inhibition by •NO, whereas CYP142 and CYP125 are more resistant to the conditions found in activated macrophages, in which •NO and O_2 are simultaneously present.

EXPERIMENTAL PROCEDURES

Materials. Econazole, glucose, glucose oxidase from *Aspergillus niger*, bovine liver catalase, and horse heart myoglobin were purchased from Sigma-Aldrich.

Molecular Cloning of cyp125, cyp142, and cyp51 Genes. Genomic DNA from *Mtb* H37Rv was obtained from the TB research materials available at Colorado State University (http://www.cvmbs.colostate.edu/microbiology/tb/materials.htm). The DNA regions encoding the putative CYP125 and CYP142 were amplified by PCR using *Pfu* Turbo DNA polymerase (Stratagene) and primers listed in Table S1 (Supporting Information). The amplification conditions were 94 °C for 5 min, 5 cycles of 94 °C for 30 s, 55 °C for 30 s, and 72 °C for 3 min followed by 25 cycles of 94 °C for 30 s, 65 °C for 30 s, and 72 °C for 3 min. The PCR program was ended by a polymerization step at 72 °C for 25 min. To confirm the DNA sequences, PCR fragments were first cloned into pCR2.1 TOPO vector (Invitrogen), and then the *Nde*I−*Hin*dIII digested fragments were subcloned into a modified pCW vector (*21*), which allows the expression of recombinant proteins with an N-terminal His_6 tag.

Expression of Mtb P450s in Escherichia coli Cells. Recombinant *Mtb* CYP51, CYP125, CYP130, and CYP142 were expressed in *E. coli* DH5α cells and purified according to a previously described protocol (*18*). The concentration of P450 was determined from difference spectra using the extinction coefficient $\epsilon_{450-490} = 91000\ M^{-1}\ cm^{-1}$ (*22*).

Anaerobic Conditions. Sample preparation for UV−vis spectroscopy and stopped-flow spectrophotometric experiments to be carried out under anaerobic conditions was performed in a glovebox (UniLab, MBraun Inc.) equipped with a catalytic purifier that maintained the oxygen content at ≤3 ppm. To reproducibly maintain satisfactorily strict anaerobic conditions, the sample-handling unit of the stopped-flow spectrophotometer was treated for at least 2 h with a glucose oxidase/catalase O_2-removing system consisting of 2 units/mL glucose oxidase, 10 mM glucose, and 130 units/mL of catalase.

Optical Absorption Spectroscopy. UV−visible absorption spectra of the purified proteins in buffer were recorded on a Cary UV−visible scanning spectrophotometer (Varian) using a 1 cm path length quartz cuvette at 23 °C. The ferric−NO species was obtained in strict anaerobic conditions as described above and by flushing the headspace of the cuvette with Ar (Airgas, CA) for 15 min followed by pure •NO gas (Matheson Tri Gas, CA) for 30 s.

Stopped-Flow Spectrophotometry. Rapid mixing experiments were conducted with a Hi-Tech Scientific instrument (Bradford on Avon, U.K.) equipped with a photodiode array detector. All of the reaction kinetics were measured at 23 °C, unless otherwise specified. Kinetic data were analyzed using the Specfit/32 program (Spectrum Software Associates, USA). The kinetic constants obtained from the fitting had uncertainties of ≤5%.

NO Combination Rate. Solutions of ferric *Mtb* P450s (5 μM) were mixed rapidly with buffered solutions of •NO (50−2000 μM), and the reaction was followed at 437 and 418 nm, a maximum and minimum, respectively, in the Fe^{3+}−NO form minus Fe^{3+} form difference spectrum. At least six •NO concentrations were used.

NO Dissociation Rate. Solutions of ferric−NO *Mtb* P450s (10 μM heme, 20 μM •NO) were mixed rapidly with a solution of ferrous−O_2 myoglobin (Mb−O_2, 25 μM). The reaction was followed by photodiode array spectroscopy over very short (0.9 s) and long (450 s) time scales. Mb−O_2 was prepared in the glovebox by reducing the ferric form with 5 mol equiv of sodium dithionite for 5 min. The ferrous deoxy protein was next passed onto a size-exclusion column (PD10; Amersham Biosciences) equilibrated with anaerobic buffer to remove excess of sodium dithionite. The eluted ferrous Mb was diluted at a final concentration of 25 μM with air-saturated buffer.

Reduction of Ferric−NO Mtb P450s with Dithionite. Solutions of ferric−NO *Mtb* P450s (5 μM heme plus 100 μM •NO) were reacted with an anaerobic solution of sodium dithionite (250 μM). A total of 200 spectra were recorded over different time scales up to 2225 s.

Resonance Raman Spectra. The equipment used to acquire the resonance Raman spectra has been described previously (*23*). The spectra of the ferrous−NO complexes were obtained with the 413 nm line of a krypton ion laser (Innova 302 laser; Coherent, Santa Clara, CA). Typically, several 1 min spectra were recorded with a low excitation power (3−4 mW) at room temperature and averaged with Grams software (ThermoGalactic, Salem, NH). The spectra were calibrated with the lines of indene in the 200−1900 cm^{-1} region. To verify the stability of the samples, optical spectra of the samples in the Raman cuvette were recorded prior to and after the resonance Raman spectra were obtained. Typically, samples containing 30−40 μM protein, based on the P450 content, were used to acquire the resonance Raman spectra.

RESULTS

Expression and Purification of CYP125 and CYP142. Using a pCW vector, the previously uncharacterized CYP125 and CYP142 proteins were expressed in *E. coli* in good

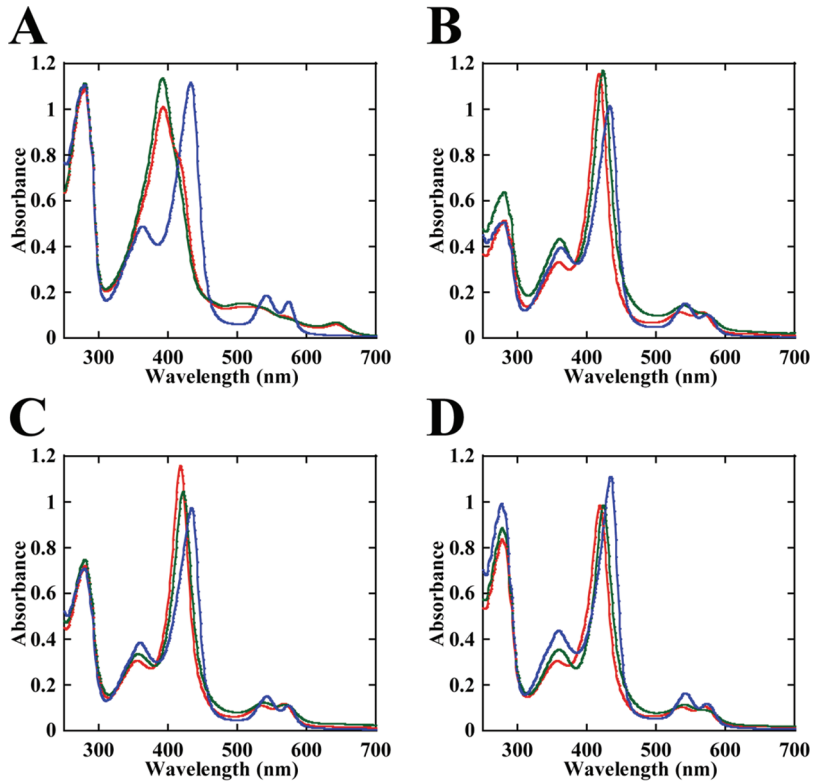

FIGURE 1: UV−visible absorption spectra of CYP125 (A), CYP142 (B), CYP130 (C), and CYP51 (D). Spectra of the resting ferric (red line), ferric−econazole (green line), and ferric−NO (blue line) forms were recorded at a protein concentration of 10 μM in 50 mM potassium phosphate buffer (pH 7.4) containing 0.1 mM EDTA at 23 °C.

yields. The proteins were purified to apparent homogeneity by Ni^{2+}-affinity and anion-exchange Q-Sepharose chromatography. The yields after purification, as estimated by P450 content, were ~125 and 1250 nmol/L of culture for CYP125 and CYP142, respectively.

UV−Visible Absorption Spectroscopy. The UV−visible absorption spectra of different ferric forms of CYP130, CYP51, and the two previously uncharacterized proteins CYP125 and CYP142 are presented in Figure 1. The resting form of CYP125 exists mostly in the high-spin state, as evidenced by a Soret band at 392 nm and the presence of a charge transfer band (CT) at 643 nm (Figure 1A). A shoulder at 419 nm indicates the presence of a small but significant fraction of low-spin heme. In contrast, CYP142, CYP130, and CYP51 were purified from *E. coli* in the ferric form with the heme iron in the low-spin state with a water molecule as the probable sixth ligand, as evidenced by a Soret band located at 418 nm and α and β bands at 567 and 535 nm, respectively (Figure 1B−D).

The addition of the antifungal azole agent econazole to all of the proteins except CYP125 resulted in the expected type II spectral shift in which the Nε1 atom of the azole group coordinates to the heme iron (Figure 1B−D). In contrast, the binding of econazole to CYP125 caused a complete transition to the high-spin state, as evidenced by sharper Soret and CT bands at 390 and 643 nm, respectively (Figure 1A). The bubbling of •NO into solutions of ferric proteins prepared under strictly anaerobic conditions resulted for all proteins in the formation of nitrosyl complexes characterized by Soret, α, and β bands located at 433, 572, and 541 nm, respectively.

NO Combination. The combination rates for •NO binding to *Mtb* CYP125, CYP130, CYP142, and CYP51 were measured by stopped-flow spectrophotometry. As a representative set of data for all four P450 enzymes, Figure 2 shows the time courses at 433 nm as a function of increasing •NO concentration for CYP51. The reactions of CYP51, CYP125, and CYP130 with •NO were nearly monophasic, and the observed pseudo-first-order rate constants increase linearly with the •NO concentration (Figure 3). On the other hand, the time course of •NO combination with CYP142 was better fitted to a double exponential function, and two distinct sets of pseudo-first-order rate constants were obtained (Figure 3C). The second-order association rate constants (k'_{on}) calculated from the slopes of these plots are summarized in Table 1. Remarkably, the k'_{on} values range from 0.2 to 17.1 μM^{-1} s^{-1}, indicating that these proteins possess very different active site architectures. The biphasic behavior of the CYP142 kinetics can be interpreted in terms of an equilibrium between CYP142 conformational substates.

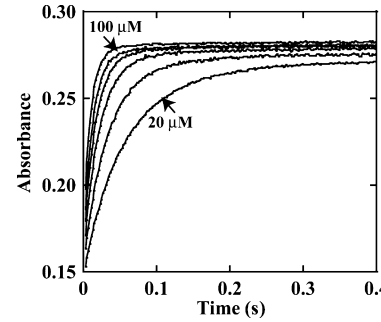

FIGURE 2: Absorbance−time plots for the binding of •NO to CYP51 recorded at 433 nm at 23 °C. Ferric CYP51 (2.5 μM final) was reacted with 20, 37.5, 50, 62.5, 75, and 100 μM •NO.

NO Dissociation. The rate of •NO dissociation for the four *Mtb* P450s was measured by mixing the ferric−NO com-

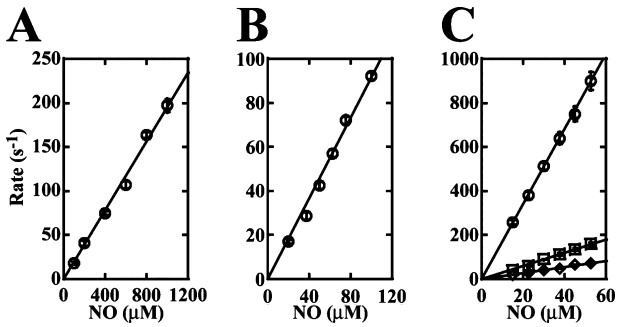

FIGURE 3: •NO concentration dependence of k_{obs} for the binding of •NO to *Mtb* CYP130 (A), CYP51 (B), and CYP125 and CYP142 (C) as measured by stopped-flow spectrophotometry. The ferric P450 enzymes (2.5 μM final) were reacted with increasing •NO concentrations at 23 °C (CYP130 and CYP51) or 10 °C (CYP125 and CYP142) in 50 mM potassium phosphate buffer (pH 7.4) containing 0.1 mM EDTA. Plots for CYP125 (circle) and the fast (square) and the slow (diamond) phases of •NO binding to CYP142 are presented in panel C.

plexes with Mb−O_2. By this approach, both free •NO and •NO released from ferric−nitrosyl complexes were instantly converted into nitrate through the NO dioxygenase activity of Mb−O_2. In a control experiment, in which Mb−O_2 was rapidly mixed with the same total concentration of free •NO, we confirmed that the scavenging action of Mb−O_2 is very efficient (>500 s^{-1}) and outcompetes the release of •NO from our four *Mtb* P450s (Figure 4, inset). The kinetics of oxidation of Mb−O_2 due to the •NO released from P450−NO complexes was monitored at 433 nm and satisfactorily fitted to a single exponential, as shown in Figure 4. The observed rates are summarized in Table 1. The k_{off} values for CYP130, CYP142, and CYP51 are higher than that of camphor-free CYP101 but are similar to that of camphor-bound CYP101. On the other hand, the k_{off} value for CYP125 is higher than that of CYP101 and approaches the value of human inducible nitric oxide synthase (iNOS).

Reduction of Ferric−NO Complex with Sodium Dithionite. We unsuccessfully attempted to measure •NO binding kinetic constants in the ferrous state in the absence of dithionite. Indeed, we first investigated the reduction of the ferric *Mtb* P450s by sodium dithionite and the stability of the resulting ferrous deoxy and ferrous−CO derivatives by stopped-flow spectrophotometry. Figures S1 and S2 (Supporting Information) present the calculated species obtained after singular value decomposition (SVD) and global analysis of the spectral data collected in the absence or presence of CO. The wavelength maxima of the different calculated species and all derived rate constants are summarized in Tables S2−S5 (Supporting Information). Although the reduction rate is very slow, CYP125 and CYP142 exhibit stable ferrous deoxy and ferrous−CO species (Figures S1 and S2, panels A and B). However, the preparation of the ferrous deoxy form of these two proteins is not only time-consuming but technically unfeasible due to the very high tendency to autoxidize after removal of the excess of sodium dithionite by gel filtration chromatography (not shown). For CYP130 and CYP51, the reduction rate is not really a limiting factor, but these two proteins exhibit moderate to high instability in the ferrous state, as evidenced by the formation of a six-coordinate (6c) low-spin and CO−P420 species in the absence and presence of CO (Figure S1 and S2, panels C and D), respectively. This phenomenon is not uncommon in P450 enzymes and has previously been reported for *Mtb* CYP51 and CYP121 (*24*).

Alternatively, we looked at the formation of ferrous−NO complexes by anaerobic reduction of the ferric−NO forms with dithionite. To capture the optical spectra of the possible intermediates in the formation of the final ferrous−NO complexes, the reaction was analyzed using a stopped-flow spectrophotometer equipped with a photodiode detector. For this, the ferric−NO proteins were reacted with dithionite (250 μM), and 200−300 spectra were collected at increasing time scales. Singular value decomposition and global analysis allowed fitting of the kinetic data for all of the proteins to models involving two, three, or even four species. For clarity, only the calculated spectra (Figure 5) and their concentration profiles are presented (Figure 5, insets). Selected representative real spectra at definite time points for all four proteins are also available and are shown in Figure S3 (Supporting Information). In addition, the wavelength maxima of all calculated species and derived rates are listed in Tables S6 and S7 (Supporting Information). As detailed below, the reduction of the ferric−NO forms of our *Mtb* P450s resulted in the formation of 5c ferrous−NO complexes characterized by a blue-shifted Soret band (389−409 nm) and a subtle peak at ~480 nm. Furthermore, the deduced affinities of our *Mtb* P450s for •NO in the ferrous state are extremely high, as evidenced by the lack of CO replacement after flushing the protein samples with Ar for 4 min to get rid of excess •NO followed by saturation of the protein solutions with 1 atm of CO (≈1 mM, at room temperature). Indeed, absolutely no replacement of •NO by CO has been observed after collecting spectral data for at least 60 min (data not shown).

CYP125. The spectral data recorded for CYP125 were fitted to the model A → B with a slow rate constant k = 0.058 s^{-1} (Table S7, Supporting Information). As shown in Figure 5A, species A matches perfectly to that of the initial ferric−NO protein, whereas species B corresponds to an unexpected ferrous−NO form characterized by a Soret band at 409 nm. Indeed, the blue-shifted Soret band strongly suggests the formation of a major 5c ferrous−NO species and not the expected 6c ferrous−NO species. The lack of detection of a more red-shifted 6c ferrous−NO species can be explained by a much faster rate of conversion from the 6c to the 5c ferrous−NO compared to that of the very slow reduction of the heme iron by sodium dithionite.

CYP142. As shown in Figure 5B, the reaction of the ferric−NO form of CYP142 with sodium dithionite was also very slow and resulted in the formation of three new species. Indeed, the spectral data can be qualitatively described with a model A → B → C, but the addition of a fourth species D gave a much better fit. Similarly to what we saw with CYP125, the reduction of the ferric−NO resulted in the formation of blue-shifted ferrous−NO complexes. Species C is similar to the ferrous−NO observed with CYP125 and is also characterized by a Soret at 409 nm, whereas species B exhibits a Soret centered at 424 nm. We propose that species B and C originate from two spectrally indistinguishable ferric−NO conformers but with different reduction kinetics. The spectral features of species D are similar those of the ferrous deoxy species described in Figure S1 (Supporting Information), indicating that the •NO bound to the protein is very slowly released and scavenged by the excess of sodium dithionite. This last observation indeed supports

Table 1: Kinetic Parameters of •NO Binding to Ferric P450 and NOS Enzymes

protein	k'_{on} (μM^{-1} s^{-1})	k_{off} (s^{-1})	K_d (μM)	ref
CYP125	17.1[a]	11.2 ± 0.1[b]	0.65	this work
CYP130	0.2	2.45 ± 0.02[b]	12.3	this work
CYP142	3.07	1.09 ± 0.01[b]	0.36	this work
	1.38		0.79	
CYP51	0.9	1.90 ± 0.02[b]	2.11	this work
CYP101 ($P450_{cam}$) camphor-free	0.32	0.35[c]	1.094	*37*
	0.0058			
CYP101 ($P450_{cam}$) camphor-bound	34.5	1.93[c]	0.0563	*37*
$P450_{nor}$	26[d]	nd		*51*
neuronal NOS (heme domain)	21	40[b]	1.905	*52*
inducible NOS (-H_4B-L-Arg)	0.059[d]	29[d,e]	491.5	*53*

[a] For *Mtb* CYP125, the k'_{on} was measured at 10 °C. [b] For these P450s, the k_{off} was measured by using Mb−O_2 as a •NO scavenger. [c] For *Pseudomonas putida* $P450_{cam}$, the k_{off} was measured by using an excess of [Ru^{III}(EDTA)H_2O] to scavenge •NO. [d] For *Fusarium oxysporum* P450nor and human iNOS, the kinetics parameters were measured at 10 °C. [e] For human iNOS, the value of the k_{off} derived from the *Y*-intercept of the plot of association rate (k_{obs}) versus [•NO].

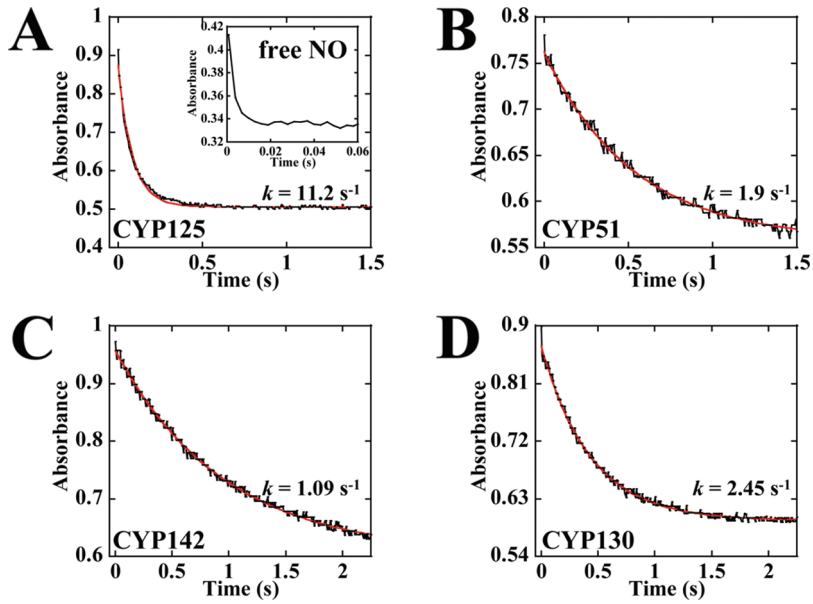

FIGURE 4: •NO dissociation from CYP125 (A), CYP130 (B), CYP142 (C), and CYP51 (D) ferric−NO complexes. Ferric−NO complexes (5 μM protein and 10 μM •NO, after mixing) prepared under strictly anaerobic conditions were reacted with an air-saturated solution of Mb−O_2 (12.5 μM, after mixing) at 23 °C. For each experiment, a total of 300 spectra were collected over time using a photodiode array detector. The reaction of oxidation of Mb−O_2 by the •NO released from P450s was well described using a single exponential function. The kinetics at 433 nm and the fit are shown.

the idea that the affinity of •NO for ferrous *Mtb* P450s is high and may inhibit the function of these enzymes *in vivo*.

CYP130. The spectral data for CYP130 were best fitted to a model A → B → C. As shown in Figure 5C, ferric−NO CYP130 (species A) is converted within 1 s to species B characterized by a red-shifted Soret band at 436 nm and a shoulder at 417 nm. B is not a pure species but is representative of a mixture of 6c ferrous−NO and ferrous deoxy species. For the next 8 s, B decayed to species C that corresponds to a 5c ferrous−NO form, as evidenced by a blue-shifted Soret band at 388 nm (*25*) and a subtle peak at ~480 nm (*26*). Moreover, the low-absorbing and broad Soret band is indicative of some heme destruction, suggesting that the holoprotein also underwent partial denaturation upon reduction.

CYP51. The kinetic data for the reduction of ferric−NO CYP51 presented in Figure 5D were fitted with a model consisting of three species. The initial ferric−NO form (species A) reacted rapidly with sodium dithionite to give a putative 5c ferrous−NO form (species B) that is spectrally similar to the 5c ferrous−NO complex of mammalian CYP1A2 characterized by a Soret band at 400 nm (*27*). This intermediate was then quickly converted to species C, characterized by a Soret band at 396 nm and a shoulder centered at ~375 nm, suggesting that CYP51, like CYP130, underwent partial denaturation and some release of heme.

Resonance Raman Spectroscopy of the Ferrous−NO Species. Resonance Raman spectroscopy was used to support the proposal that the ferrous−NO complexes of our *Mtb* P450 enzymes are mostly or completely 5c. The resonance Raman spectra of the ferrous−NO complexes of CYP130 and CYP51 (Figure 6A,B) recorded in the high-frequency region show υ_4, υ_3, and υ_{10} lines at 1375, 1508, and 1645 cm^{-1}, respectively. The frequencies of these lines are indicative of a typical 5c ferrous−NO species (*25, 28*). Furthermore, the binding of NO to the heme iron is confirmed by the high frequency of the υ_4 line (1375 cm^{-1}). A shoulder at ≈1360−1362 cm^{-1} is assigned to photodissociated products based on the identical frequencies displayed by the υ_4 line of the ferrous 6c low-spin form of CYP130 and CYP51 obtained after the reduction of ferric enzymes by sodium dithionite (Raman spectra not shown and Figure S1). On the

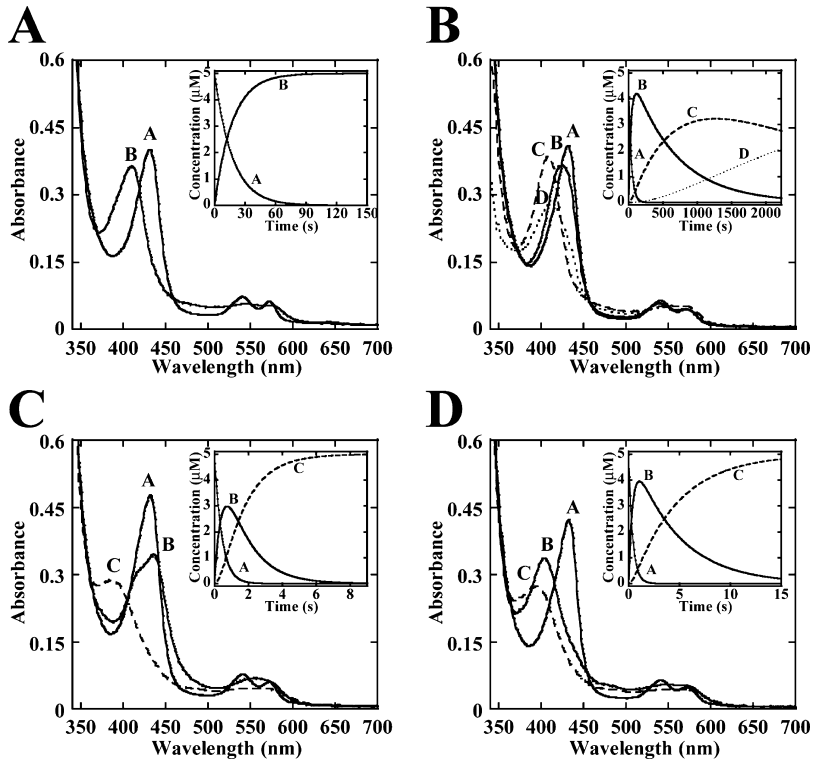

FIGURE 5: Reduction of *Mtb* P450 ferric−nitrosyl complexes by sodium dithionite. Calculated spectra obtained from SVD and global analysis of the data recorded for CYP125 (A), CYP142 (B), CYP130 (C), and CYP51 (D). Ferric−nitrosyl complexes (5 μM protein and 100 μM •NO, after mixing) prepared under strictly anaerobic conditions were reacted with sodium dithionite (250 μM, after mixing) at 23 °C. For each experiment, a total of 300 spectra were collected over time using the photodiode array detector. The wavelength maxima of the derived species and the calculated rates are summarized in Tables S6 and S7 (Supporting Information), respectively.

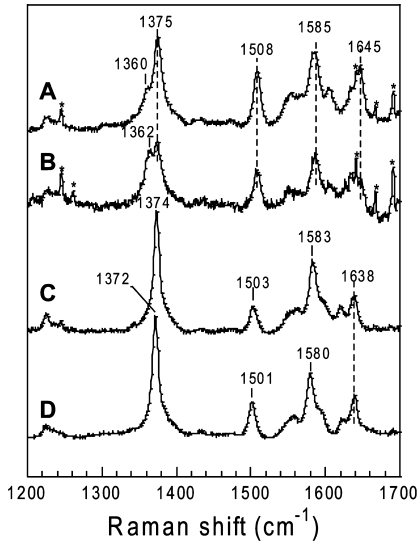

FIGURE 6: High-frequency region of the resonance Raman spectra of the ferrous−NO complexes of CYP130 (A), CYP51 (B), CYP125 (C), and CYP142 (D). All spectra were recorded at 23 °C in 50 mM potassium phosphate buffer (pH 7.4) containing 0.1 mM EDTA. For CYP142 the spectrum was recorded only after completion of the reduction reaction. Stars correspond to laser lines.

other hand, the resonance Raman spectra of CYP125 and CYP142 (Figures 6C,D) exhibit υ_4, υ_3, and υ_{10} lines at ~1373, ~1502, and 1638 cm^{-1}, respectively. The frequencies of the υ_3 and υ_{10} lines are different from those of a typical 5c ferrous−NO complex, near 1508 cm^{-1} (υ_3) and near 1645 cm^{-1} (υ_{10}) (*28, 29*), respectively. The υ_3 line is also different from those of 6c ferrous−NO species of thiolate-coordinated heme proteins, which are typically in the 1497−1499 cm^{-1} range (*25, 30, 31*). The observed frequencies are similar to those displayed by nNOS Trp409 mutants (*25*), which rather suggests a mixture that contains a majority of a 5c ferrous−NO and a minority of a 6c ferrous−NO species that may not retain the thiolate ligand (*32*).

Reaction of the Ferrous−NO Complexes with O_2. As mentioned earlier, the lack of replacement of •NO by CO indicates that the affinity of the ferrous state for •NO is extremely high and predicts that •NO would be a better inhibitor of P450 activity than CO. Therefore, to address the stability of the ferrous−NO complexes under aerobic conditions, we mixed anaerobically prepared NO-bound protein solutions with a buffer solution saturated with O_2. Before exposure to O_2, the protein samples were first flushed with Ar to remove excess •NO, thus limiting the potential for chemical modifications of the protein by reactive nitrogen products. Spectra were collected at 1 min intervals for different periods of time, and the data are shown in Figure S4 (Supporting Information). For CYP142, exposure of the 5c ferrous−NO complex to O_2 resulted in relatively fast conversion (less than 7 min) to the ferric state (Figure S4, panel B, Supporting Information). The oxidation of the ferrous−NO form of CYP125 was even faster and was complete within 2 min (not shown). In contrast, the ferrous−NO complexes of CYP130 and CYP51 reacted very slowly with O_2, resulting in the formation of only 10% of ferric protein after 12 h (Figure S4, panel A, Supporting Information). Altogether, these results suggest that the two classes of 5c ferrous−NO complexes have different reactivities. Consequently, the binding of •NO to the ferrous protein, or reduction of the ferric−NO complex, would result

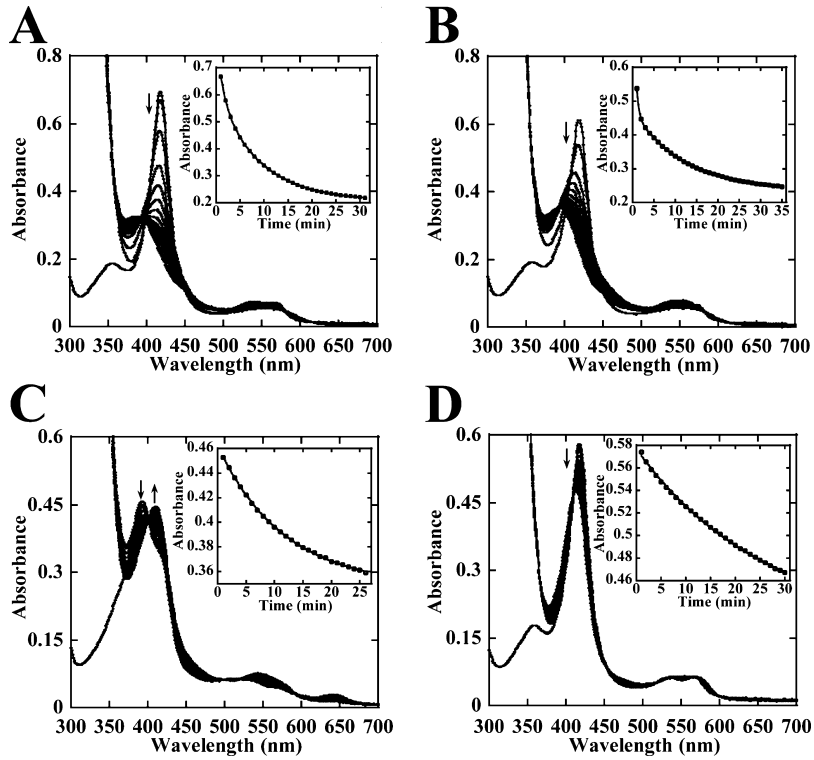

FIGURE 7: Nitrite reductase activity of *Mtb* CYP130 (A), CYP51 (B), CYP125 (C), and CYP142 (D). The ferric proteins (5 μM) were prepared under strictly anaerobic conditions in the presence of a physiological concentration of nitrite (100 μM). The reaction was initiated by the addition of ≈500 μM sodium dithionite. Spectra were recorded every minute up to 25−35 min at 23 °C. Insets: Time courses at 417 nm for CYP130, CYP51, and CYP142 and at 390 nm for CYP125. A nitrite reductase activity was observed for CYP130 and CYP51, as evidenced by the formation of their respective 5c ferrous−NO species, whereas CYP125 and CYP142 are slowly converted to their respective ferrous deoxy form.

in quasi-irreversible inhibition of CYP130 and CYP51 but in reversible inhibition of CYP125 and CYP142.

Nitrite Reductase Activity. •NO is proposed to play an important role in controlling the growth of *Mtb* in its human host but also induces an adaptation program that allows the mycobacteria to survive in a dormant state. •NO is very unstable, and nitrate is one of the stable breakdown end products, suggesting that when *Mtb* cells enter into dormancy, nitrate is available. Furthermore, induction of nitrate reduction activity was recently shown to enhance the survival of *Mtb* cells during inhibition of aerobic respiration (*33*). One possible dark side of this enhanced nitrate reductase activity would be the release of the more reactive product, nitrite. Indeed, acidification and enzymatic reduction of nitrite lead to a significant production of •NO. The latter mechanism has been recently shown to be of physiological relevance, as exemplified by the nitrite reductase activity of ferrous myoglobin and its role in the regulation of mitochondrial respiration and blood circulation (*34, 35*).

We thus investigated the possibility that *Mtb* P450 enzymes might be self-inhibited by •NO generated under hypoxic conditions by a nitrite reductase activity. Ferric *Mtb* P450 enzymes were incubated with a physiological concentration of nitrite (100 μM) under strictly anaerobic conditions. The reduction reactions were triggered by the addition of 0.5 mM sodium dithionite. As shown in Figure 7A,B, CYP130 and CYP51 were progressively converted into their respective 5c ferrous−NO forms, as evidenced by the increase of absorbance at 387 or 395 nm. In the case of CYP125 and CYP142, we did not observe any formation of ferrous−NO but only a slow conversion to their respective ferrous deoxy form (Figure 7C,D). For these two proteins, the lack of accumulation of ferrous−NO complex can be explained by a faster destruction of •NO by sodium dithionite compared to its formation due to a too slow reduction of the heme (Figure S1, Supporting Information). These results suggest that (1) heme−thiolate proteins, like imidazole−heme proteins, are capable of •NO formation by virtue of a nitrite reductase activity and (2) nitrite accumulation in *Mtb* cells during hypoxia can constitute an autocatalytically generated source of •NO that could interfere with normal P450 activities.

DISCUSSION

•NO is a small gas molecule that can bind to both ferric and ferrous forms of heme−containing enzymes, and several lines of evidence indicate that P450 enzymes might be targeted by •NO *in vivo*. Here, we have studied the interactions between •NO and four *Mtb* P450 enzymes, CYP125, CYP130, CYP142, and CYP51. Of these, we report the first expression and initial characterization of CYP125 and CYP142. We have used UV−visible absorption spectroscopy and stopped-flow spectrophotometry to investigate the binding of •NO to these enzymes in their ferric resting state and the reduction of the resulting ferric−NO complexes with sodium dithionite. We have also explored the self-inhibition of these enzymes by virtue of a previously undetected nitrite reductase activity that generates •NO.

Binding of •NO to the Ferric Form. As shown by the data in Table 1, •NO binds to the ferric, substrate-free forms of CYP125, CYP142, and CYP51 and CYP101 with compa-

rable affinities ($K_d \leq 2\ \mu M$). This range of concentrations is in good accordance with the steady-state concentrations of •NO measured in activated macrophages (*36*). Although CYP130 exhibits a higher K_d value (Table 1) in the ferric state, its affinity presumably increases dramatically when the heme iron is in its reduced form, as suggested by the resistance of the ferrous−NO complex to oxidation (Figure S4, Supporting Information) and replacement by CO (not shown).

The rates of combination of •NO with our four *Mtb* P450s are in good agreement with previous values obtained for other thiolate-ligated heme proteins, including $P450_{cam}$, CYP1A2, and NOS (Table 1). Indeed, the anionic nature of the proximal thiolate ligand stabilizes the ferric state and increases dramatically the reactivity toward •NO compared to that of imidazole-ligated heme proteins like myoglobin (*37*). However, all of these thiolate-ligated proteins still exhibit a wide range of combination rate constants, indicating that other factors also affect the reaction. One of these factors is the increased lability of the leaving water molecule that is coordinated to the heme. Accordingly, CYP125, which exhibits a much higher content of high-spin heme in its resting state, showed by far the fastest •NO combination reaction. Moreover, the presence of substrate in the active site has also been shown to negatively affect the dynamics of the reaction with gas ligands by making the protein and the heme pocket more rigid (*38*). Since we do not know the natural substrate(s) for our enzymes, such comparisons cannot be made here.

Ferrous−Nitrosyl Complexes. A very high affinity for ferric enzymes contributes only in part to the full inhibitory potential of •NO. Indeed, as opposed to the coordination of type II ligands that tend to be inhibitors because they stabilize the low reduction potential of P450 and prevent heme reduction and O_2 binding (*39*), the binding of •NO tends to facilitate reduction of the heme group. We have shown here that reduction of the ferric−nitrosyl forms of the *Mtb* P450s carried out chemically does not give rise to formation of stable 6c ferrous−NO species but rather to two distinct classes of 5c ferrous−nitrosyl complexes with different reactivities toward O_2. Indeed, with the exception of a very small amount of 6c ferrous−NO complex detected with CYP130, no kinetic evidence for the accumulation of a stable 6c ferrous−NO intermediate was observed by UV−visible absorption spectrophotometry, indicating that the Fe−S bond is very labile. Resonance Raman spectroscopy data support the idea that CYP130 and CYP51 form typical 5c ferrous−NO complexes (Figure 6A,B). Indeed, comparisons with other thiolate-ligated proteins strongly suggest that the ferrous−NO complexes of CYP130 and CYP51 are identical to those of the mammalian CYP1A2, substrate-free nNOS, the heme−thiolate sensor CooA from *Rhodospirillum rubrum*, the human heme-containing eIF2α kinase, and nitrophorin of the bloodsucking insect *Cimex lectularius* (Table S8, Supporting Information) (*25, 40−42*). For the latter protein, structural data confirmed that the Fe−Cys bond was broken and an S−NO adduct was formed with the released proximal Cys (*40*). It was also shown that the 6c ferrous−NO complex of wild-type nNOS is stable only in the presence of H_4B or L-arginine; in their absence, the initial 6c ferrous−NO complex converts with time to a 5c ferrous−NO complex characterized by wavelength maxima at 394 and ∼570 nm (*25*). So far, identification of the natural substrate for any *Mtb* P450 remains elusive; however, it is likely that substrate-bound enzymes have altered heme pocket structures that presumably reinforce the proximal thiolate bond and consequently may result in more stable 6c ferrous−NO complexes.

In contrast, the ferrous−nitrosyl complexes of CYP125 and CYP142 are more similar to those observed for the substrate- and cofactor-bound complexes of the W409F and W409Y mutants of nNOS with a more red-shifted Soret band at 409 nm. The Trp residue at position 409 is conserved in all NOS isoforms. The crystal structure data show that the indole nitrogen atom of this Trp residue forms an H-bond with the sulfur atom of the proximal Cys ligand (*43, 44*). Resonance Raman (*25*) and magnetic circular dichroism spectroscopy (*32*) indicated that the ferrous−NO complexes of these proteins consist of a mixture of major 5c and minor 6c species. By the use of resonance Raman spectroscopy we also obtained quite similar results for CYP125 and CYP142. Interestingly, it was shown that changing Trp409 to either Phe or Tyr resulted in more active nNOS enzymes (*45*). This was later explained by the fact that the two mutants do not form as much heme−NO complex during catalysis due to faster decay of their ferrous−NO back to the ferric form in the presence of O_2 (*46*). Similarly, we observed a higher reactivity of the ferrous−NO species of CYP125 and CYP142 toward O_2, suggesting that the activity of these two enzymes would be less impaired *in vivo*, compared to that of CYP130 and CYP51.

Physiological Sources of •NO. The major source of •NO responsible for the induction and maintenance of bacilli dormancy in activated macrophages is proposed to be iNOS. In the murine tuberculosis model, it has been shown that genetic disruption of iNOS results in higher risk of dissemination and mortality after infection with *Mtb* (*47, 48*). The role of •NO in killing *Mtb* in human cells is more controversial, but there is a growing body of evidence supporting the involvement of •NO and iNOS (*2, 49*). However, the enzymatic activity of NOS requires oxygen and would be impaired at the low O_2 concentrations presumably found in the granuloma. In this context, it was shown recently that endothelial NOS (eNOS) possesses a nitrite reductase activity capable of delivering •NO in hypoxic vascular tissues (*50*). We show here that CYP130 and CYP51 and potentially other thiolate-ligated heme proteins reduce physiological concentrations of nitrite to •NO. This was clearly evidenced by the trapping of •NO by the heme, leading to the formation of ferrous−NO complexes.

Conclusions. A role for •NO in the inhibition of P450 activities in dormant *Mtb* cells is conceivable. However, so far, genomic and proteomic studies have not reported any significant impact of cell exposure to •NO on P450 levels at either the mRNA or protein levels. Instead, the present results suggest that •NO inhibition may be mediated by the direct formation of heme−NO adducts. Indeed, we show that at least three members of the *Mtb* P450 complement bind •NO in their ferric state with high affinities. Moreover, the reduction of the ferric−nitrosyl complexes resulted, for CYP130 and CYP51, in the formation of quasi-irreversible 5c ferrous−NO species that barely convert back to the ferric state upon reexposure to O_2. In contrast, the ferrous−NO complexes of CYP125 and CYP142 are more labile, indicat-

ing that these two enzymes are less susceptible to inhibition. Furthermore, we show that at least two *Mtb* P450s enzymes are capable of reducing nitrite ions to •NO, resulting in an autoinhibitory process.

SUPPORTING INFORMATION AVAILABLE

The list of PCR primers for the cloning of *cyp* genes studied here (Table S1), spectral data from the reduction of ferric P450 enzymes by sodium dithionite in the absence or presence of CO (Figures S1 and S2), the wavelength maxima of the calculated spectra and kinetic rates obtained from the reduction of the ferric and ferric−nitrosyl derivatives by sodium dithionite (Tables S2−S7), selected representive real spectra from the reduction of the ferric−NO complexes by sodium dithionite (Figure S3), the wavelength maxima of the electronic absorption spectra of the ferric− and ferrous−nitrosyl complexes of selected thiolate-ligated heme proteins (Table S8), a list of relevant references (Table S8), and the oxidation of ferrous−nitrosyl complexes in the presence of O_2 (Figure S4). This material is available free of charge via the Internet at http://pubs.acs.org.

REFERENCES

1. Toossi, Z., and Ellner, J. J. (2000) Pathogenesis of tuberculosis. *Tuberculosis: Current Concepts and Treatment*, 19–47.
2. Chan, E. D., Chan, J., and Schluger, N. W. (2001) What is the role of nitric oxide in murine and human host defense against tuberculosis? Current knowledge. *Am. J. Respir. Cell Mol. Biol. 25*, 606–612.
3. Flynn, J. L., and Chan, J. (2003) Immune evasion by *Mycobacterium tuberculosis*: living with the enemy. *Curr. Opin. Immunol. 15*, 450–455.
4. Long, R., Light, B., and Talbot, J. A. (1999) Mycobacteriocidal action of exogenous nitric oxide. *Antimicrob. Agents Chemother. 43*, 403–405.
5. Gow, A. J., Foust, R., Malcolm, S., Gole, M., and Ischiropoulos, H. (1999) Biochemical regulation of nitric oxide toxicity. *Nitric Oxide and Infection*, 175–187.
6. Brunori, M. (2001) Nitric oxide, cytochrome-*c* oxidase and myoglobin. *Trends Biochem. Sci. 26*, 21–23.
7. Pfeiffer, S., Gorren, A. C., Schmidt, K., Werner, E. R., Hansert, B., Bohle, D. S., and Mayer, B. (1997) Metabolic fate of peroxynitrite in aqueous solution. Reaction with nitric oxide and pH-dependent decomposition to nitrite and oxygen in a 2:1 stoichiometry. *J. Biol. Chem. 272*, 3465–3470.
8. Nathan, C., and Shiloh, M. U. (2000) Reactive oxygen and nitrogen intermediates in the relationship between mammalian hosts and microbial pathogens. *Proc. Natl. Acad. Sci. U.S.A. 97*, 8841–8848.
9. Alexander, B. (1998) The role of nitric oxide in hepatic metabolism. *Nutrition 14*, 376–390.
10. Donato, M. T., Guillen, M. I., Jover, R., Castell, J. V., and Gomez-Lechon, M. J. (1997) Nitric oxide-mediated inhibition of cytochrome P450 by interferon-gamma in human hepatocytes. *J. Pharmacol. Exp. Ther. 281*, 484–490.
11. Cole, S. T., Brosch, R., Parkhill, J., Garnier, T., Churcher, C., Harris, D., Gordon, S. V., Eiglmeier, K., Gas, S., Barry, C. E., III, Tekaia, F., Badcock, K., Basham, D., Brown, D., Chillingworth, T., Connor, R., Davies, R., Devlin, K., Feltwell, T., Gentles, S., Hamlin, N., Holroyd, S., Hornsby, T., Jagels, K., Krogh, A., McLean, J., Moule, S., Murphy, L., Oliver, K., Osborne, J., Quail, M. A., Rajandream, M. A., Rogers, J., Rutter, S., Seeger, K., Skelton, J., Squares, R., Squares, S., Sulston, J. E., Taylor, K., Whitehead, S., and Barrell, B. G. (1998) Deciphering the biology of *Mycobacterium tuberculosis* from the complete genome sequence. *Nature 393*, 537–544.
12. McLean, K. J., and Munro, A. W. (2008) Structural biology and biochemistry of cytochrome P450 systems in *Mycobacterium tuberculosis*. *Drug Metab. Rev. 40*, 427–446.
13. Bellamine, A., Mangla, A. T., Nes, W. D., and Waterman, M. R. (1999) Characterization and catalytic properties of the sterol 14alpha-demethylase from *Mycobacterium tuberculosis*. *Proc. Natl. Acad. Sci. U.S.A. 96*, 8937–8942.
14. Van der Geize, R., Yam, K., Heuser, T., Wilbrink, M. H., Hara, H., Anderton, M. C., Sim, E., Dijkhuizen, L., Davies, J. E., Mohn, W. W., and Eltis, L. D. (2007) A gene cluster encoding cholesterol catabolism in a soil actinomycete provides insight into *Mycobacterium tuberculosis* survival in macrophages. *Proc. Natl. Acad. Sci. U.S.A. 104*, 1947–1952.
15. Chang, J. C., Harik, N. S., Liao, R. P., and Sherman, D. R. (2007) Identification of mycobacterial genes that alter growth and pathology in macrophages and in mice. *J. Infect. Dis. 196*, 788–795.
16. Rengarajan, J., Bloom, B. R., and Rubin, E. J. (2005) Genome-wide requirements for *Mycobacterium tuberculosis* adaptation and survival in macrophages. *Proc. Natl. Acad. Sci. U.S.A. 102*, 8327–8332.
17. Leys, D., Mowat, C. G., McLean, K. J., Richmond, A., Chapman, S. K., Walkinshaw, M. D., and Munro, A. W. (2003) Atomic structure of *Mycobacterium tuberculosis* CYP121 to 1.06 A reveals novel features of cytochrome P450. *J. Biol. Chem. 278*, 5141–5147.
18. Ouellet, H., Podust, L. M., and de Montellano, P. R. (2008) *Mycobacterium tuberculosis* CYP130: crystal structure, biophysical characterization, and interactions with antifungal azole drugs. *J. Biol. Chem. 283*, 5069–5080.
19. Seward, H. E., Roujeinikova, A., McLean, K. J., Munro, A. W., and Leys, D. (2006) Crystal structure of the *Mycobacterium tuberculosis* P450 CYP121-fluconazole complex reveals new azole drug-P450 binding mode. *J. Biol. Chem. 281*, 39437–39443.
20. Podust, L. M., Poulos, T. L., and Waterman, M. R. (2001) Crystal structure of cytochrome P450 14alpha-sterol demethylase (CYP51) from *Mycobacterium tuberculosis* in complex with azole inhibitors. *Proc. Natl. Acad. Sci. U.S.A. 98*, 3068–3073.
21. Gegner, J. A., and Dahlquist, F. W. (1991) Signal transduction in bacteria: CheW forms a reversible complex with the protein kinase CheA. *Proc. Natl. Acad. Sci. U.S.A. 88*, 750–754.
22. Omura, T., and Sato, R. (1964) The carbon monoxide-binding pigment of liver microsomes. I. Evidence for its hemoprotein nature. *J. Biol. Chem. 239*, 2370–2378.
23. Chartier, F. J., and Couture, M. 2004) Stability of the heme environment of the nitric oxide synthase from *Staphylococcus aureus* in the absence of pterin cofactor. *Biophys. J. 87*, 1939–1950.
24. McLean, K. J., Dunford, A. J., Sabri, M., Neeli, R., Girvan, H. M., Balding, P. R., Leys, D., Seward, H. E., Marshall, K. R., and Munro, A. W. (2006) CYP121, CYP51 and associated redox systems in *Mycobacterium tuberculosis*: towards deconvoluting enzymology of P450 systems in a human pathogen. *Biochem. Soc. Trans. 34*, 1178–1182.
25. Couture, M., Adak, S., Stuehr, D. J., and Rousseau, D. L. (2001) Regulation of the properties of the heme-NO complexes in nitric-oxide synthase by hydrogen bonding to the proximal cysteine. *J. Biol. Chem. 276*, 38280–38288.
26. Yoshimura, T., and Ozaki, T. (1984) Electronic spectra for nitrosyl(protoporphyrin IX dimethyl ester)iron(II) and its complexes with nitrogenous bases as model systems for nitrosylhemoproteins. *Arch. Biochem. Biophys. 229*, 126–135.
27. Nakano, R., Sato, H., Watanabe, A., Ito, O., and Shimizu, T. (1996) Conserved Glu318 at the cytochrome P450 1A2 distal site is crucial in the nitric oxide complex stability. *J. Biol. Chem. 271*, 8570–8574.
28. Lukat-Rodgers, G. S., and Rodgers, K. R. (1997) Characterization of ferrous FixL-nitric oxide adducts by resonance Raman spectroscopy. *Biochemistry 36*, 4178–4187.
29. Couture, M., Burmester, T., Hankeln, T., and Rousseau, D. L. (2001) The heme environment of mouse neuroglobin. Evidence for the presence of two conformations of the heme pocket. *J. Biol. Chem. 276*, 36377–36382.
30. Deng, T. J., Proniewicz, L. M., Kincaid, J. R., Yeom, H., Macdonald, I. D., and Sligar, S. G. (1999) Resonance Raman studies of cytochrome P450BM3 and its complexes with exogenous ligands. *Biochemistry 38*, 13699–13706.
31. Hu, S., and Kincaid, J. R. (1991) Resonance Raman spectra of the nitric oxide adducts of ferrous cytochrome P450cam in the presence of various substrates. *J. Am. Chem. Soc. 113*, 9760–9766.
32. Voegtle, H. L., Sono, M., Adak, S., Pond, A. E., Tomita, T., Perera, R., Goodin, D. B., Ikeda-Saito, M., Stuehr, D. J., and Dawson, J. H. (2003) Spectroscopic characterization of five- and six-coordinate ferrous-NO heme complexes. Evidence for heme Fe-proximal cysteinate bond cleavage in the ferrous-NO adducts of

the Trp-409Tyr/Phe proximal environment mutants of neuronal nitric oxide synthase. *Biochemistry 42*, 2475–2484.
33. Sohaskey, C. D. (2008) Nitrate enhances the survival of *Mycobacterium tuberculosis* during inhibition of respiration. *J. Bacteriol. 190*, 2981–2986.
34. Hendgen-Cotta, U. B., Merx, M. W., Shiva, S., Schmitz, J., Becher, S., Klare, J. P., Steinhoff, H. J., Goedecke, A., Schrader, J., Gladwin, M. T., Kelm, M., and Rassaf, T. (2008) Nitrite reductase activity of myoglobin regulates respiration and cellular viability in myocardial ischemia-reperfusion injury. *Proc. Natl. Acad. Sci. U.S.A. 105*, 10256–10261.
35. Shiva, S., Huang, Z., Grubina, R., Sun, J., Ringwood, L. A., MacArthur, P. H., Xu, X., Murphy, E., Darley-Usmar, V. M., and Gladwin, M. T. (2007) Deoxymyoglobin is a nitrite reductase that generates nitric oxide and regulates mitochondrial respiration. *Circ. Res. 100*, 654–661.
36. Lewis, R. S., Tamir, S., Tannenbaum, S. R., and Deen, W. M. (1995) Kinetic analysis of the fate of nitric oxide synthesized by macrophages *in vitro*. *J. Biol. Chem. 270*, 29350–29355.
37. Franke, A., Stochel, G., Jung, C., and Van Eldik, R. (2004) Substrate binding favors enhanced NO binding to P450cam. *J. Am. Chem. Soc. 126*, 4181–4191.
38. Jung, C., Bec, N., and Lange, R. (2002) Substrates modulate the rate-determining step for CO binding in cytochrome P450cam (CYP101). A high-pressure stopped-flow study. *Eur. J. Biochem. 269*, 2989–2996.
39. Locuson, C. W., Hutzler, J. M., and Tracy, T. S. (2007) Visible spectra of type II cytochrome P450-drug complexes: evidence that "incomplete" heme coordination is common. *Drug Metab. Dispos. 35*, 614–622.
40. Weichsel, A., Maes, E. M., Andersen, J. F., Valenzuela, J. G., Shokhireva, T., Walker, F. A., and Montfort, W. R. (2005) Heme-assisted S-nitrosation of a proximal thiolate in a nitric oxide transport protein. *Proc. Natl. Acad. Sci. U.S.A. 102*, 594–599.
41. Igarashi, J., Sato, A., Kitagawa, T., Yoshimura, T., Yamauchi, S., Sagami, I., and Shimizu, T. (2004) Activation of heme-regulated eukaryotic initiation factor 2alpha kinase by nitric oxide is induced by the formation of a five-coordinate NO-heme complex: optical absorption, electron spin resonance, and resonance Raman spectral studies. *J. Biol. Chem. 279*, 15752–15762.
42. Reynolds, M. F., Parks, R. B., Burstyn, J. N., Shelver, D., Thorsteinsson, M. V., Kerby, R. L., Roberts, G. P., Vogel, K. M., and Spiro, T. G. (2000) Electronic absorption, EPR, and resonance Raman spectroscopy of CooA, a CO-sensing transcription activator from *R. rubrum*, reveals a five-coordinate NO-heme. *Biochemistry 39*, 388–396.
43. Fischmann, T. O., Hruza, A., Niu, X. D., Fossetta, J. D., Lunn, C. A., Dolphin, E., Prongay, A. J., Reichert, P., Lundell, D. J., Narula, S. K., and Weber, P. C. (1999) Structural characterization of nitric oxide synthase isoforms reveals striking active-site conservation. *Nat. Struct. Biol. 6*, 233–242.
44. Crane, B. R., Arvai, A. S., Ghosh, D. K., Wu, C., Getzoff, E. D., Stuehr, D. J., and Tainer, J. A. (1998) Structure of nitric oxide synthase oxygenase dimer with pterin and substrate. *Science 279*, 2121–2126.
45. Adak, S., Crooks, C., Wang, Q., Crane, B. R., Tainer, J. A., Getzoff, E. D., and Stuehr, D. J. (1999) Tryptophan 409 controls the activity of neuronal nitric-oxide synthase by regulating nitric oxide feedback inhibition. *J. Biol. Chem. 274*, 26907–26911.
46. Adak, S., Wang, Q., and Stuehr, D. J. (2000) Molecular basis for hyperactivity in tryptophan 409 mutants of neuronal NO synthase. *J. Biol. Chem. 275*, 17434–17439.
47. Adams, L. B., Dinauer, M. C., Morgenstern, D. E., and Krahenbuhl, J. L. (1997) Comparison of the roles of reactive oxygen and nitrogen intermediates in the host response to *Mycobacterium tuberculosis* using transgenic mice. *Tuberc. Lung Dis. 78*, 237–246.
48. MacMicking, J. D., North, R. J., LaCourse, R., Mudgett, J. S., Shah, S. K., and Nathan, C. F. (1997) Identification of nitric oxide synthase as a protective locus against tuberculosis. *Proc. Natl. Acad. Sci. U.S.A. 94*, 5243–5248.
49. Nicholson, S., Bonecini-Almeida Mda, G., Lapa e Silva, J. R., Nathan, C., Xie, Q. W., Mumford, R., Weidner, J. R., Calaycay, J., Geng, J., Boechat, N., Linhares, C., Rom, W., and Ho, J. L. (1996) Inducible nitric oxide synthase in pulmonary alveolar macrophages from patients with tuberculosis. *J. Exp. Med. 183*, 2293–2302.
50. Gauthier, C., van Faassen, E., Mikula, I., Martasek, P., and Slama-Schwok, A. (2006) Endothelial nitric oxide synthase reduces nitrite anions to NO under anoxia. *Biochem. Biophys. Res. Commun. 341*, 816–821.
51. Shiro, Y., Fujii, M., Iizuka, T., Adachi, S., Tsukamoto, K., Nakahara, K., and Shoun, H. (1995) Spectroscopic and kinetic studies on reaction of cytochrome P450nor with nitric oxide. Implication for its nitric oxide reduction mechanism. *J. Biol. Chem. 270*, 1617–1623.
52. Scheele, J. S., Bruner, E., Kharitonov, V. G., Martasek, P., Roman, L. J., Masters, B. S., Sharma, V. S., and Magde, D. (1999) Kinetics of NO ligation with nitric-oxide synthase by flash photolysis and stopped-flow spectrophotometry. *J. Biol. Chem. 274*, 13105–13110.
53. Abu-Soud, H. M., Wu, C., Ghosh, D. K., and Stuehr, D. J. (1998) Stopped-flow analysis of CO and NO binding to inducible nitric oxide synthase. *Biochemistry 37*, 3777–3786.

BI801595T